X-ray magnetic circular dichroism and photoemission studies of ferromagnetism in $CaMn_{1-x}Ru_xO_3$ thin films

K. Terai, K. Yoshii, Y. Takeda, S. I. Fujimori, Y. Saitoh, K. Ohwada, T. Inami, and T. Okane
Synchrotron Radiation Research Unit, Japan Atomic Energy Agency, SPring-8, Sayo-gun, Hyogo 679-5148, Japan

M. Arita, K. Shimada, H. Namatame, and M. Taniguchi
Hiroshima Synchrotron Radiation Center, Hiroshima University, Kagamiyama, Higashi-Hiroshima 739-0046, Japan

K. Kobayashi
National Institute for Materials Science, SPring-8, Sayo-gun, Hyogo 679-5148, Japan

M. Kobayashi and A. Fujimori
Department of Physics, University of Tokyo, Bunkyo-ku, Tokyo 113-0033, Japan
(Received 19 March 2007; revised manuscript received 28 January 2008; published 19 March 2008)

We have studied the electronic and magnetic properties of epitaxially grown $CaMn_{1-x}Ru_xO_3$ thin films ($x=1.0, 0.75, 0.5$) by soft x-ray absorption, soft x-ray magnetic circular dichroism (XMCD), and hard x-ray photoemission spectroscopy (HXPES) measurements. The XMCD studies indicated that the spin moments of Mn and Ru are aligned in opposite directions. The valence-band HXPES spectra revealed that the Ru $4d$ t_{2g} states around the Fermi level and the Mn $3d$ t_{2g} up-spin states centered ~ 2 eV below it showed systematic concentration dependences. From these results, we propose that the localized Mn $3d$ t_{2g} states and the itinerant Ru $4d$ t_{2g} band are antiferromagnetically coupled and give rise to the ferromagnetic ordering, which is in analogy to the mechanism proposed for double perovskite oxides, such as Sr_2FeMoO_6.

DOI: 10.1103/PhysRevB.77.115128 PACS number(s): 75.47.Lx, 75.50.Cc, 75.70.−i, 78.70.Dm

I. INTRODUCTION

Perovskite-type ruthenium oxides show various interesting physical properties, such as the triplet superconductivity in Sr_2RuO_4 (Ref. 1) and the itinerant ferromagnetism in $SrRuO_3$.[2,3] Ferromagnetic correlations among the itinerant Ru $4d$ electrons are considered to play a critical role in causing these properties. In the paramagnetic metal $CaRuO_3$ (CRO), substitution of a small amount of magnetic Fe, Mn, and Ni or nonmagnetic Ti for Ru induces ferromagnetism.[4] In particular, the pseudobinary alloy system $CaMn_{1-x}Ru_xO_3$ (CMRO) shows ferromagnetism with the maximum transition temperature T_c (150–210 K) and the maximum magnetic moment at $x \simeq 0.5$.[4,5] Both end members are not, however, ferromagnetic; that is, $CaMnO_3$ (CMO) is a G-type antiferromagnetic insulator[6] and CRO is a paramagnetic metal.[7] The origin of ferromagnetism in CMRO with $x<0.5$ has been explained by a double exchange mechanism between Mn^{4+} and Mn^{3+}, where Mn^{3+} ions are created when Ru atoms are replaced by Mn atoms.[4] However, this explanation needs charge transfer from Ru to Mn, which seems difficult considering the higher electronegativity of Ru than that of Mn. CMO and CRO superlattices have also been shown to exhibit ferromagnetism.[8] The total magnetic moment of superlattices does not depend on the thickness of layers, but only on the number of interfaces, suggesting that ferromagnetism occurs in the interfaces between the CRO and CMO layers.

In order to understand the unique physical properties of CMRO, it is important to obtain information about the electronic structure and its relationship to ferromagnetism. Photoemission spectroscopy and x-ray absorption spectroscopy (XAS) are useful methods to investigate the electronic structure of solids. Conventional photoemission spectroscopy, in which the photon energy is less than ~ 1 keV, is sensitive to the surface region because the probing depth of photoexcited electrons is less than ~ 10 Å in this electron kinetic energy range. On the other hand, hard x-ray photoemission spectroscopy (HXPES) has the great advantage of bulk sensitivity due to the large probing depth of photoelectrons of several nanometers. Soft x-ray magnetic circular dichroism (XMCD) using the core-level absorption process is an element specific probe sensitive to the magnetic moments of each element and, therefore, is a powerful experimental method for the investigation of magnetism in complex materials. Another advantage of XMCD is its capability to separately evaluate the spin and orbital magnetic moments. Recently, high quality single-crystal thin films with atomically flat surfaces have been grown by the pulsed laser deposition (PLD) method. This method is one of the most promising sample fabrication methods for electron spectroscopy measurements,[9,10] such as XAS, XMCD, and photoemission spectroscopy. In this paper, we have fabricated CMRO thin films by using the PLD method and studied their electronic structure by using HXPES and XAS and their magnetic properties by using XMCD. The results of these measurements showed systematic dependences of the electronic and magnetic properties on Mn concentration.

II. EXPERIMENT

Epitaxial CMRO ($x=1.0, 0.75, 0.5$) thin films were fabricated by the PLD method. Sintered ceramics of $CaMnO_3$ and $CaRuO_3$ were used as ablation targets. Sample concentra-

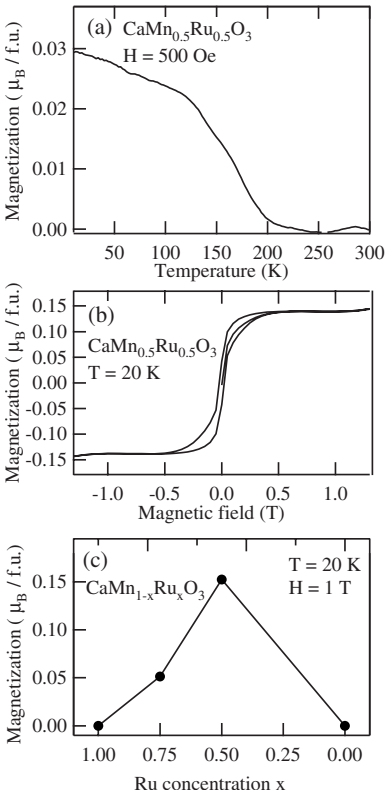

FIG. 1. Magnetic properties of $CaMn_{0.5}Ru_{0.5}O_3$ thin films for magnetic fields applied perpendicular to the sample surface. (a) Temperature dependence of the magnetization measured at 500 Oe showing the transition temperature of ~200 K. (b) Magnetization curves for the same thin film measured at 20 K, showing a hysteresis loop. (c) Ru concentration dependence of the magnetization of $CaMn_{1-x}Ru_xO_3$.

tions were controlled by the laser pulse ratio. $LaAlO_3$ (100) single crystals were used as substrates, which had been annealed at 900 °C prior to deposition. The oxygen pressure was 10^{-6} Torr during the substrate annealing. A Nd:YAG (where YAG denotes yttrium aluminum garnet) laser was used for ablation in the frequency-tripled mode (λ =355 nm) with a repetition rate of 1 Hz. The oscillation of the reflection high-energy electron diffraction intensity during the film growth indicated that the growth was made in a layer-by-layer mode. The CMRO thin films with 200 Å thickness were deposited on the substrates at 700 °C at an oxygen pressure of 1×10^{-4} Torr. The fabricated samples were quickly transferred through the atmosphere to the XMCD chamber. The sample surface morphology was checked by *ex situ* atomic force microscopy (AFM). The AFM image showed straight steps and terraces, which means that our thin films provided a smooth surface for photoemission spectroscopy.

The magnetization of the samples was measured by a superconducting quantum interference device (SQUID) magnetometer before the measurements of XAS and XMCD. Figure 1(a) shows the temperature dependence of the magnetization of the CMRO (x=0.5) thin film under a magnetic field applied perpendicular to the sample surface. The figure shows $T_c \sim 200$ K in the thin film. As shown in the

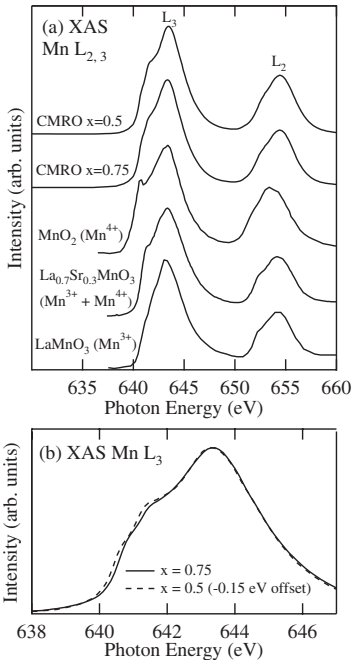

FIG. 2. (a) Mn $L_{2,3}$ XAS spectra of $CaMn_{1-x}Ru_xO_3$ (x =0.5,0.75) thin films compared with those of MnO_2, $La_{0.7}Sr_{0.3}MnO_{7-\delta}$ (Ref. 15), and $LaMnO_3$ (Ref. 16), which are reference materials for Mn^{4+}, Mn^{3+}, and Mn^{3+}+Mn^{4+}, respectively. (b) Magnified plot of the Mn L_3 XAS spectra of CMRO (x=0.5,0.75). The spectrum of CMRO (x=0.5) has been shifted by −0.15 eV for comparison.

hysteresis curve of CMRO (x=0.5) in Fig. 1(b), the magnetization saturates above ~0.5 T to ≃0.15 μ_B/f.u. at 20 K. Figure 1(c) shows the concentration dependence of the maximum magnetization at 20 K, which is consistent with the largest magnetization for $x \simeq 0.5$ in the previous report on bulk samples.[4,5]

The XAS and XMCD measurements were performed at BL23-SU of SPring-8.[11] Spectra were recorded by the total electron yield method. XMCD spectra were obtained by reversing the photon helicity at each photon energy. The degree of circular polarization of the x rays was determined by polarization measurements using a Cr/Sc multilayer detector,[12] and was estimated to be greater than 90% at 400 eV. An external magnetic field was applied perpendicular to the thin film surfaces. The measurements were performed at 20 K under the external magnetic field of 2 T. The HXPES measurements[13,14] were performed at BL22-XU of SPring-8. The sample temperature was 30 K during the measurements. The total energy resolution was about 270 meV at a photon energy of 3.5 keV. The position of the Fermi level (E_F) was determined by measuring gold spectra.

III. RESULTS

A. Mn 3*d* $L_{2,3}$-edge x-ray absorption spectroscopy

Figure 2(a) shows the Mn $L_{2,3}$ XAS spectra of CMRO (x=0.5,0.75). The spectra show a multiplet structure, suggesting that the Mn 3*d* electrons have a strongly localized

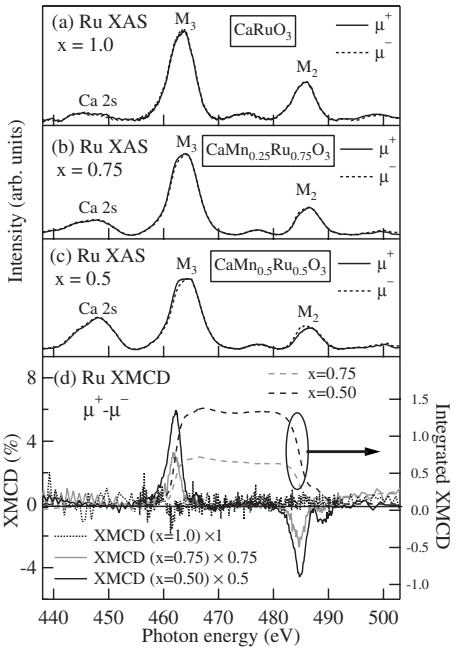

FIG. 3. Concentration dependence of (a) XAS and (b) XMCD spectra at the Mn $L_{2,3}$ edges. The XAS spectra have been normalized to the peak height of the corresponding XAS spectra. The XMCD spectra have been normalized to the peak height of the corresponding XAS spectra. The measurements were performed at 20 K under a magnetic field of 2 T.

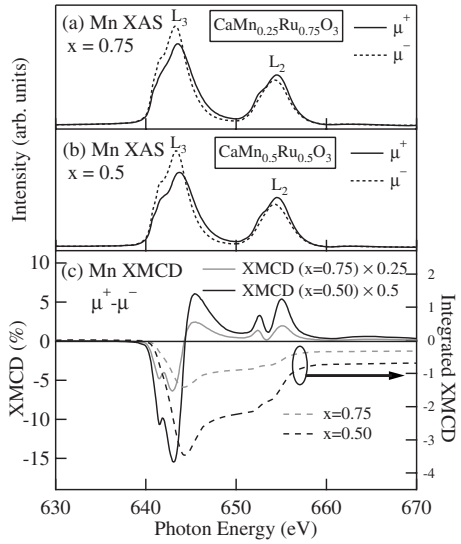

FIG. 4. Concentration dependence of (a) XAS and (b) XMCD spectra at the Ru $M_{2,3}$ edges. The spectra have been normalized in the same way as the Mn $L_{2,3}$. The measurements were performed at 20 K under a magnetic field of 2 T.

character as in typical Mn compounds in the literature.[15,16] The spectral line shape of CMRO is different from that of $LaMnO_3$ (Mn^{3+}) but is similar to those of MnO_2 (Mn^{4+}) and $La_{0.7}Sr_{0.3}MnO_{7-\delta}$ ($Mn^{3+}+Mn^{4+}$). Therefore, the Mn atoms in CMRO are considered to be in the tetravalent state 4+ or in a mixed-valence state of 3+ and 4+. Figure 2(b) shows a magnified plot of the Mn L_3 XAS spectra of CMRO ($x=0.5,0.75$). The spectrum of CMRO ($x=0.5$) has been shifted by −0.15 eV for comparison. The left shoulder of Mn L_3 for $x=0.5$ is slightly larger than that for $x=0.75$. On the other hand, it was difficult to determine the Ru valence from the Ru $L_{2,3}$ XAS spectrum because the spectrum showed a broad line shape due to the itinerant nature of the Ru 4d electrons.

B. X-ray magnetic circular dichroism

Figures 3 and 4 show the XAS spectra and the XMCD spectra of the Mn $L_{2,3}$ ($2p \rightarrow 3d$) and Ru $M_{2,3}$ ($3p \rightarrow 4d$) absorption edges normalized to the corresponding XAS peak intensity. The structure of the Ca 2s core level more rapidly increased than the chemical compositions imply as the Mn concentration increased, as shown in Figs. 3(b) and 3(c). It may suggest that more excess Ca atoms were segregated as impurity phases as the Mn concentration increased. The XMCD spectra were obtained as the differences of the XAS spectra, $\mu^+ - \mu^-$, where μ^+ and μ^- denote the XAS spectra measured with right-handed and left-handed circularly polarized light, respectively. The XMCD spectra have been normalized to the peak height of the corresponding XAS spectra. The XMCD signal for $x=0.5$ was the strongest among the studied concentrations, which is consistent with the magnetization measurements shown in Fig. 1. The sign of the Ru $M_{2,3}$ XMCD signal was opposite that of the Mn $L_{2,3}$ XMCD, indicating that the direction of the Ru 4d magnetic moment is opposite that of the Mn 3d magnetic moment.

Quantitatively, the spin and orbital magnetic moments of the Mn and Ru atoms were estimated as follows by using the XMCD sum rules:[17,18]

$$M_{\text{orbital}} = -\frac{4}{3}\frac{\int_{L_3+L_2[M_3+M_2]} (\mu^+ - \mu^-)d\omega}{\int_{L_3+L_2[M_3+M_2]} (\mu^+ + \mu^-)d\omega}(10 - N_d),$$

$$M_{\text{spin}} + 7M_T = -\frac{2\int_{L_3[M_3]} (\mu^+ - \mu^-)d\omega - 4\int_{L_2[M_2]} (\mu^+ - \mu^-)d\omega}{\int_{L_3+L_2[M_3+M_2]} (\mu^+ + \mu^-)d\omega} \times (10 - N_d).$$

Here, M_{orbital} and M_{spin} are the orbital and spin magnetic moments in units of μ_B/atom, respectively. The magnetic dipole moment M_T was neglected for simplicity because it was estimated to be small (less than 1% of M_{spin}) in the ligand-field theoretical calculation of 3d tradition elements.[19] N_d is the d electron occupation number, which was assumed to be 3 to 4 both for Ru 4d and Mn 3d. The XAS spectra in Fig. 2 indicate a mixed-valence state of 3+ and 4+, which implies that the N_d of Mn is intermediate between 3 and 4. Because one cannot precisely estimate the valence of Mn from the XAS spectra, M_{orbital} and M_{spin} were calculated

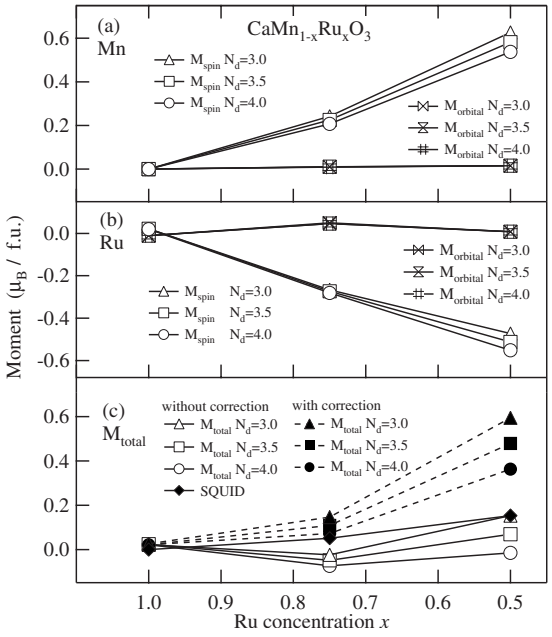

FIG. 5. Spin and orbital moments of the (a) Mn and (b) Ru atoms as functions of Ru concentration x. N_d of Mn is assumed to be 4, 3.5, and 3 in the calculations using the sum rules. (c) The total magnetic moment from XMCD has been derived as described in the text. Filled and empty symbols show results with and without a correction factor, respectively.

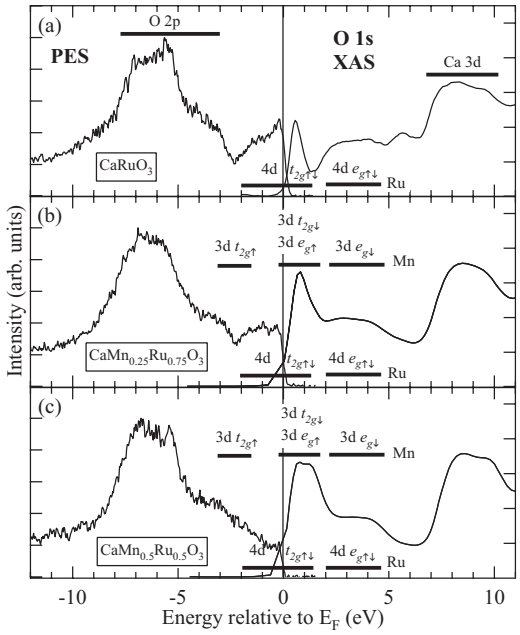

FIG. 6. Combined plot of the valence-band HXPES spectra and the O $1s$ XAS spectra of CMRO (x=1.0, 0.75, 0.5).

using the sum rule under different assumptions of N_d(Mn) =3, 3.5, and 4. As for Ru, we assume $N_d(\mathrm{Ru})=[(3+x)-(1-x)N_d(\mathrm{Mn})]/x$.

Figures 5(a) and 5(b) show the concentration dependence of M_{orbital} and M_{spin} of Mn or Ru, in units of μ_B/f.u. One can see that M_{orbital} is only 0.01 μ_B/f.u. for Ru and 0.03 μ_B/f.u. for Mn at x=0.5. The small M_{orbital} is consistent with the Mn^{4+} state.[20] M_{spin} for both elements linearly increases with decreasing Ru concentration.

Figure 5(c) shows the concentration dependence of the total magnetic moment calculated from M_{orbital} and M_{spin}. In the case of x=0.5 and N_d(Mn)=3.5, the Mn and Ru spin moments were estimated to be 0.58 and −0.51 μ_B/f.u., respectively. Therefore, the total magnetic moment was estimated to be 0.07 μ_B/f.u. However, the magnetic moment of Mn calculated using the sum rules contained an error due to the L_2-L_3 mixing. Teramura *et al.*[19] discussed this problem and derived correction factors for various transition metals. Because the correction factor for Mn^{3+} was not reported, the correction factors for Mn^{4+} (0.587) have been used here. Therefore, the total magnetic moment per f.u. is estimated to be $0.48\mu_B$ [=(0.58/0.587)−0.51]. A wide-range scan of x-ray photoemission spectroscopy measurements indicated that Ca concentration increased with Mn concentration. It is possible that the decrease in total magnetic moments in our film was caused by this nonstoichiometry.

C. Valence-band hard x-ray photoemission spectroscopy and O 1*s* x-ray absorption spectroscopy

Figure 6 shows a combined plot of the valence-band HXPES spectra and the O $1s$ XAS spectra of CMRO (x=1.0, 0.75, 0.5), representing the electronic state below and above E_F. The position of the Fermi level of the HXPES and XAS spectra has been determined by the Au $4f$ positions for each measurement. The HXPES and XAS spectra have been normalized to the intensity of the O $2p$ and Ca $3d$ bands, respectively.

The intensity of the structure near E_F in the HXPES spectra decreased as the concentration of Ru decreased. At the same time, the intensity of the structure near E_F in the XAS spectra increased as the Mn concentration increased. These structures are attributed to the Ru $4d$ t_{2g} states because the previous band-structure calculations[21,22] and photoemission measurement[23] on CRO have indicated that the Ru $4d$ t_{2g} states are located near E_F. The occupied Ru $4d$ states were more clearly observed than in the previous study,[23] which implies that we succeeded in measuring a dominantly bulk electronic structure. The band between −8 and −3 eV is mainly composed of O $2p$ states. The peak intensities of the two peak structures between around −5 and −8 eV changed with the Ru concentrations. These peaks can be assigned to the Ru-O (−5.5 eV) and Mn-O (−7 eV) bonding states. This assignment was made based on the cross sections of the Ru $4d$ and Mn $3d$ orbitals, which are relatively larger than those of the O $2p$ orbitals for the high photon energy $h\nu$ =3.5 keV. On the other hand, the peak intensity at around −3 eV did not depend on the Ru/Mn ratio and, thus, can be assigned to O $2p$ nonbonding states. These peak positions were consistent with the previous report.[23] The intensity of the structure at around −2.5 eV increased as the Mn concentration increased. Hence, the structure can be attributed to Mn $3d$ t_{2g} up-spin states by a comparison to the previous calculation.[24] By the same token, the peak structures at around 0–2 eV above E_F can be assigned to the Mn $3d$ t_{2g} down-spin and Mn $3d$ e_g up-spin states. The concentration dependence of the peak structure around 0–2 eV would be

caused by the overlap between the hybridized O 2*p*-Ru 4*d* states and the hybridized O-Mn 3*d* states.

IV. DISCUSSION

The antiferromagnetic coupling between the magnetic moments of Mn and Ru observed by XMCD cannot be explained by the conventional double exchange mechanism, which has been used to explain the ferromagnetism in the Mn perovskite systems.[25,26] Furthermore, the Ru spin moment increases with Mn concentrations. This indicates the existence of Ru 4*d*-Mn 3*d* spin coupling. The concentration dependence of XAS [Fig. 2(b)] shows that the change of the Mn valence is very small. This implies that the double exchange model is inadequate for the CMRO system.

Instead, we consider that the antiferromagnetic coupling can be explained by a model proposed for half-metallic double perovskite systems, such as Sr_2FeMoO_6 (Refs. 27 and 28) and A_2CrWO_6 (A=Sr, Ba, and Ca),[29] at least in the Ru-rich region. In the case of Sr_2FeMoO_6, the spin moments of Fe and Mo are aligned in the antiparallel directions.[30] The Fe $L_{2,3}$ XAS spectra have implied that the Fe electrons are in the localized trivalent states and that the Mo electrons are itinerant.[27] Recently, a similar mechanism has been proposed for the ferromagnetism in the pyrochlore-type $Tl_2Mn_2O_7$,[31] where the Mn atoms are in the Mn^{4+} state. These behaviors are similar to the present CMRO case, where the Mn 3*d* t_{2g} electrons are basically localized and the Ru 4*d* t_{2g} electrons are itinerant, as demonstrated by the photoemission spectra. In addition, the proximity of the Ru 4*d* t_{2g} electrons in CRO to ferromagnetism may enhance the ferromagnetic instability.[5]

The electronic structure that induces the Mn-Ru antiferromagnetic coupling discussed above is schematically shown in Fig. 7. The density of states is influenced by the Mn t_{2g}-Ru t_{2g} hybridization. In order to explain the magnetic coupling between the Mn and Ru atoms, we consider that the hybridization between neighboring Mn and Ru atoms is important. Due to the Ru 4*d*-Mn 3*d* hybridization, the Ru t_{2g} up-spin states are pushed up, while the Mn t_{2g} up-spin states are pushed down. Consequently, the antiparallel spin polarization at the Ru and Mn sites is induced due to the half-filled Mn t_{2g} states; thus, the ferromagnetic coupling is induced between the Mn atoms. The electronic structure described above is important to realize the ferromagnetism in CMRO despite the absence of ferromagnetism in both end compositions. The success of the similar models to explain the ferromagnetism in $Tl_2Mn_2O_7$ and CMRO may suggest that the model is applicable to other ferromagnetic oxides of complex perovskite type such as the Cu-Re perovskites.[32]

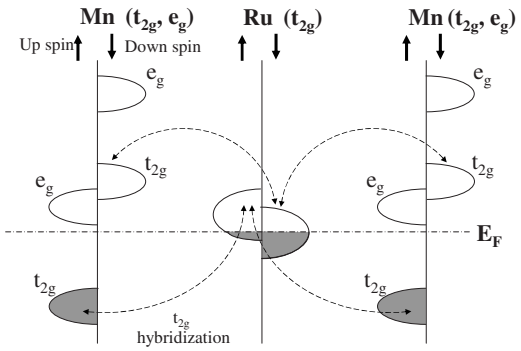

FIG. 7. Schematic of a mechanism stabilizing the antiparallel alignment of the magnetic moments between the Ru and Mn atoms. This model was used in Refs. 27–29 to describe the antiferromagnetic coupling between Fe and Mo or between Cr and W in the half-metallic double perovskites Sr_2FeMoO_3 and Sr_2CrWO_3. The inherent ferromagnetic instability of the Ru 4*d* t_{2g} band in $CaRuO_3$ may also contribute in order to stabilize the ferromagnetic spin polarization in CMRO.

V. CONCLUSION

We have performed XAS and XMCD studies on epitaxial thin films of $CaMn_{1-x}Ru_xO_3$ grown by the PLD method. The Mn $L_{2,3}$ and Ru $M_{2,3}$ XMCD spectra indicated that the orbital magnetic moments on Mn and Ru were almost quenched and that the spin moments of Mn and Ru were aligned in the antiparallel directions. Therefore, we consider that the small total magnetic moment of $CaMn_{1-x}Ru_xO_3$ results from the cancellation of the Ru and Mn spin moments. The O 1*s* XAS and valence-band HXPES indicate a clear concentration dependence of the valence-band structures that originated from the Ru 4*d* and Mn 3*d* states near E_F.

Our results do not exclude the double exchange model as a possible mechanism of ferromagnetism in CMRO. Nevertheless, the Ru spin moment increases with Mn concentrations, clearly indicating a Ru 4*d*-Mn 3*d* spin coupling. On the other hand, the present results can be explained by a model analogous to that proposed for the half-metallic double perovskite systems.[27–29] We suggest that the antiparallel coupling of the spin moments between the Mn 3*d* and Ru 4*d* electrons and, hence, the ferromagnetic coupling between the Mn 3*d* electrons in $CaMn_{1-x}Ru_xO_3$ are the origin of the ferromagnetism.

ACKNOWLEDGMENTS

Helpful discussions with T. Nomura were greatly appreciated. This work was partially supported by a Grant-in-Aid for Scientific Research from the Japan Society for the Promotion of Science (A16204024).

[1] Y. Maeno, H. Hashimoto, K. Yoshida, S. Nishizaki, T. Fujita, J. G. Bednorz, and F. Lichtenberg, Nature (London) **372**, 532 (1994).
[2] F. Fukunaga and N. Tsuda, J. Phys. Soc. Jpn. **63**, 3798 (1994).
[3] T. He, Q. Huang, and R. J. Cava, Phys. Rev. B **63**, 024402 (2000).
[4] A. Maignan, C. Martin, M. Hervieu, and B. Raveau, Solid State Commun. **117**, 377 (2001).
[5] T. He and R. J. Cava, J. Phys.: Condens. Matter **13**, 8347 (2001).
[6] E. O. Wollan and W. C. Koehler, Phys. Rev. **100**, 545 (1955).
[7] G. L. Catchen, T. M. Rearick, and D. G. Schlom, Phys. Rev. B **49**, 318 (1994).
[8] K. S. Takahashi, M. Kawasaki, and Y. Tokura, Appl. Phys. Lett. **79**, 1324 (2001).
[9] H. Kumigashira, K. Horiba, H. Ohguchi, K. Ono, M. Oshima, N. Nakagawa, M. Lippmaa, M. Kawasaki, and H. Koinuma, Appl. Phys. Lett. **82**, 3430 (2003).
[10] H. Wadati, D. Kobayashi, H. Kumigashira, K. Okazaki, T. Mizokawa, A. Fujimori, K. Horiba, M. Oshima, N. Hamada, M. Lippmaa, M. Kawasaki, and H. Koinuma, Phys. Rev. B **71**, 035108 (2005).
[11] J. Okamoto, K. Mamiya, S.-I. Fujimori, T. Okane, Y. Saitoh, Y. Muramatsu, A. Fujimori, S. Ishikawa, and M. Takano, *Eighth International Conference on Synchrotron Radiation Instrumentation*, AIP Conf. Proc. No. 705 (AIP, New York, 2004), p. 1110.
[12] H. Kimura, T. Hirono, Y. Saitoh, and T. Imazono (unpublished).
[13] K. Kobayashi, M. Yabashi, Y. Takata, T. Tokushima, S. Shin, K. Tamasaku, D. Miwa, T. Ishikawa, H. Nohira, T. Hattori, Y. Sugita, O. Nakatsuka, A. Sakai, and S. Zaima, Appl. Phys. Lett. **83**, 1005 (2003).
[14] Y. Takata, K. Tamasaku, T. Tokushima, D. Miwa, S. Shin, T. Ishikawa, M. Yabashi, K. Kobayashi, J. J. Kim, T. Yao, T. Yamamoto, M. Arita, H. Namatame, and M. Taniguchi, Appl. Phys. Lett. **84**, 4310 (2004).
[15] S. Stadler, Y. U. Idzerda, Z. Chen, S. B. Ogale, and T. Venkatesan, Appl. Phys. Lett. **75**, 3384 (1999).
[16] C. Mitra, Z. Hu, P. Raychaudhuri, S. Wirth, S. I. Csiszar, H. H. Hsieh, H.-J. Lin, C. T. Chen, and L. H. Tjeng, Phys. Rev. B **67**, 092404 (2003).
[17] B. T. Thole, P. Carra, F. Sette, and G. van der Laan, Phys. Rev. Lett. **68**, 1943 (1992).
[18] P. Carra, B. T. Thole, M. Altarelli, and X. Wang, Phys. Rev. Lett. **70**, 694 (1993).
[19] Y. Teramura, A. Tanaka, and T. Jo, J. Phys. Soc. Jpn. **65**, 1053 (1996).
[20] T. Koide, H. Miyauchi, J. Okamoto, T. Shidara, T. Sekine, T. Saitoh, A. Fujimori, H. Fukutani, M. Takano, and Y. Takeda, Phys. Rev. Lett. **87**, 246404 (2001).
[21] G. Santi and T. Jarlborg, J. Phys.: Condens. Matter **9**, 9563 (1997).
[22] I. I. Mazin and D. J. Singh, Phys. Rev. B **56**, 2556 (1997).
[23] J. Park, S.-J. Oh, J.-H. Park, D. M. Kim, and C.-B. Eom, Phys. Rev. B **69**, 085108 (2004).
[24] G. Zampieri, F. Prado, A. Caneiro, J. Briático, M. T. Causa, M. Tovar, B. Alascio, M. Abbate, and E. Morikawa, Phys. Rev. B **58**, 3755 (1998).
[25] P. Mandal and S. Das, Phys. Rev. B **56**, 15073 (1997).
[26] Y. Moritomo, A. Asamitsu, H. Kuwahara, and Y. Tokura, Nature (London) **380**, 141 (1996).
[27] D. D. Sarma, P. Mahadevan, T. Saha-Dasgupta, S. Ray, and A. Kumar, Phys. Rev. Lett. **85**, 2549 (2000).
[28] Z. Fang, K. Terakura, and J. Kanamori, Phys. Rev. B **63**, 180407(R) (2001).
[29] J. B. Philipp, P. Majewski, L. Alff, A. Erb, R. Gross, T. Graf, M. S. Brandt, J. Simon, T. Walther, W. Mader, D. Topwal, and D. D. Sarma, Phys. Rev. B **68**, 144431 (2003).
[30] M. Besse, V. Cros, A. Barthélémy, H. Jaffrès, J. Vogel, F. Petroff, A. Mirone, A. Tagliaferri, P. Bencok, P. Decorse, P. Berthet, Z. Szotek, W. M. Temmerman, S. S. Dhesi, N. B. Brookes, A. Rogalev, and A. Fert, Europhys. Lett. **60**, 608 (2002).
[31] T. Saha-Dasgupta, Molly De Raychaudhury, and D. D. Sarma, Phys. Rev. Lett. **96**, 087205 (2006).
[32] X. Wan, M. Kohno, and X. Hu, Phys. Rev. Lett. **95**, 146602 (2005).